



## ISTITUTO NAZIONALE DI RICERCA METROLOGICA Repository Istituzionale

Design and metrological evaluation of the new 5 MN hexapod-shaped multicomponent build-up system

This is the author's submitted version of the contribution published as:

*Original*

Design and metrological evaluation of the new 5 MN hexapod-shaped multicomponent build-up system / Palumbo, Stefano; Germak, ALESSANDRO FRANCO LIDIA; Mazzoleni, Fabrizio; Desogus, Sergio; Barbato, Giulio. - In: METROLOGIA. - ISSN 0026-1394. - 53:3(2016), pp. 956-964. [10.1088/0026-1394/53/3/956]

*Availability:*

This version is available at: 11696/52641 since: 2021-03-08T19:28:59Z

*Publisher:*

IOP

*Published*

DOI:10.1088/0026-1394/53/3/956

*Terms of use:*

This article is made available under terms and conditions as specified in the corresponding bibliographic description in the repository

*Publisher copyright*

Institute of Physics Publishing Ltd (IOP)

IOP Publishing Ltd is not responsible for any errors or omissions in this version of the manuscript or any version derived from it. The Version of Record is available online at DOI indicated above

(Article begins on next page)

# DESIGN AND METROLOGICAL EVALUATION OF THE NEW 5 MN HEXAPOD-SHAPED MULTICOMPONENT BUILD-UP SYSTEM

Stefano Palumbo <sup>1</sup>, Alessandro Germak <sup>2</sup>, Fabrizio Mazzoleni <sup>3</sup>, Sergio Desogus <sup>4</sup>, Giulio Barbato <sup>5</sup>

<sup>1</sup> INRIM, Torino, Italy, s.palumbo@inrim.it

<sup>2</sup> INRIM, Torino, Italy, a.germak@inrim.it

<sup>3</sup> INRIM, Torino, Italy, f.mazzoleni@inrim.it

<sup>4</sup> INRIM, Torino, Italy, s.desogus@inrim.it

<sup>5</sup> Politecnico di Torino, Italy, giulio.barbato@polito.it

**Abstract.** The new 5 MN Hexapod-Shaped Multicomponent Build-Up System (HSM-BUS) represents a significant progress in the field of reference transducers in the high force range. As any build-up system, the presented hexapod-shaped multicomponent force transducer can lead not only to measure forces 5 times higher than the capacity of a each single Uniaxial Force Transducer (UFT), but gives also information about the other components of the force vector and of the moment vector. Furthermore, the calibration of such type of multicomponent force transducer regards only the calibration of the signal outputs coming from each UFT and the calibration of the geometry of the system. In this work an a-priori evaluation of the expected uncertainty is performed. As a first approximation, the effects of the calibration uncertainties of UFTs and of the geometrical tolerances given on the construction drawing were considered. Subsequently, with a Finite Element Simulation of the mechanical behavior of the 5 MN HSM-BUS under load, a mathematical model of elastic deformations has been evaluated and applied for evaluating and correcting the systematic errors due to the deformation of the geometry under load.

**Keywords:** hexapod, load simulation, build-up system, force transducer, uncertainty budget

## 1 Introduction

The need to have traceable force calibration machines with high capacity, leads to the realization of the Build-Up System (BUS). Such systems are composed by several Uniaxial Force Transducers (UFTs) that can be calibrated directly by primary force standard machines. Generally, a BUS is composed by three UFTs [1,6] in the same direction, therefore allowing the measurement of a force that is three times the capacity of the single UFT. If it is required to reach higher loads starting from the same UFT capacity, to maintain isostatic condition, it is necessary to create a more complex structure adding additional UFTs in order to increase the total capacity [7]. Another possibility is to use a hexapod structure that use six UFTs, reaching five times the capacity of the system (considering the mounting angles), as it was already developed at INRiM [8,9]. This structure has also the advantage to allow the measurements of all the six components (Multicomponent Force Transducer, MFT), i.e. not only the principal axial force ( $F_z$ ), but also all force and moment vectors (transversal,  $F_x$  and  $F_y$ ), and three moment components, (tilting,  $M_x$  and  $M_y$ , and torsion,  $M_z$ ). The main aim is to measure the force in a given direction, in our case  $F_z$ , therefore the accuracy on all other force and moment components is not at the same metrological level. Nevertheless, the information given by the measurement of all the components can be used to get a better accuracy on the  $F_z$  measurements.

To assure traceable measurements in this type of BUS, the force calibration of UFTs is not sufficient, since the output measurements also depends on the geometry of the hexapod structure. Therefore, consideration of the

geometry and its possible variations described by the geometrical tolerances and elastic distortion under load have become necessary.

## 2 HSM-BUS Design

### 2.1 System Geometry

The system geometry of the new 5 MN HS-BU can be briefly outlined with the views of the XY-plane and of XZ-plane. In the first view (left of figure 1) we can see the distribution of the UFTs, the radius  $r$  and the angle  $\gamma$  (while angle  $\delta$  is complementary to it). In the second view (right part of figure 1), the two functional angles  $\alpha$  and  $\beta$  are shown.

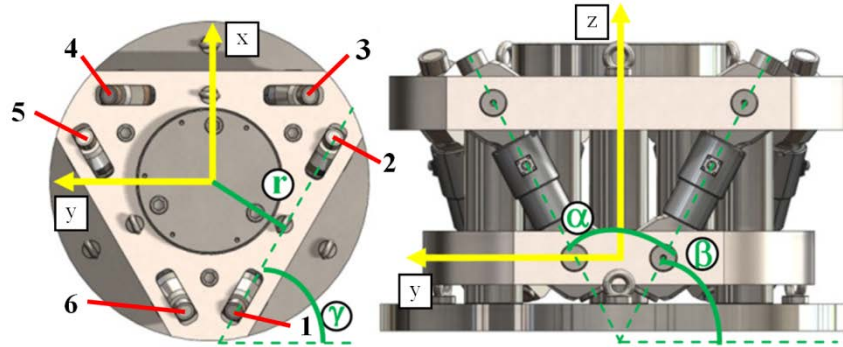


Figure 1: The geometry of MFT

As it can be seen in Fig. 1, due to dimensional limits, it was not possible to connect two UFTs into the same point; so, instead of a triangle, each pair of UFTs creates a trapezoid.

### 2.2 MFT design

The 5 MN HS-BU is designed to work with a nominal force value of 5 MN, using 6 UFTs with rated load of 1 MN, in order to be calibrated using the 1MN deadweight primary force standard machine at INRiM.

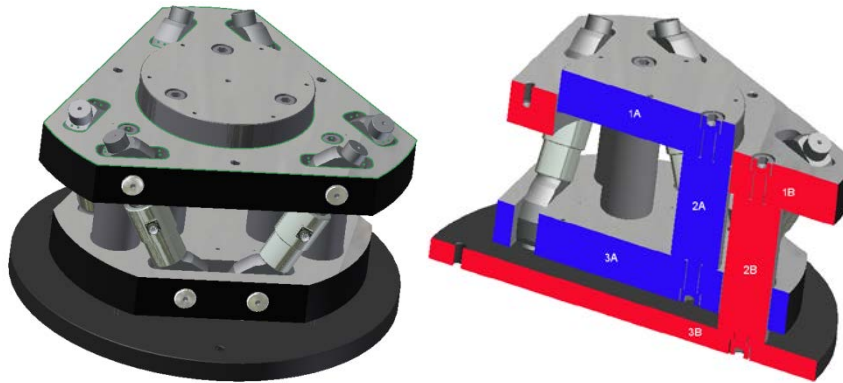


Figure 2: The 5 MN hexapod-shaped MFT

Since the UFTs have to work in traction, and not in compression as the HS-BU, it was necessary to create an inversion frame, in order to put in traction the UFTs. The load, applied on the upper loading pad (1A), is transferred by three columns (2A) to the lower plate (3A), where are fixed the lower clamping heads of the UFTs. The upper clamping heads of the UFTs are instead fixed to the upper plate (1B) which, through three columns (2B), is supported by the base (3B). To avoid any contact and frictions during the load application, frame A and frame B are spaced by a gap of some millimeters.

### 2.3 Uniaxial Force Transducers

A MFT is composed by several uniaxial force transducers (figures 1, 2). Usually, in a BUS, the number of these UFTs is three to realize an isostatic structure, although is possible to use more of them. In a HSM-BUS, indeed, are used six UFTs (figure 3a), realizing a pseudo-isostatic structure.

Another peculiarity of the HSM-BUS, is that its UFTs work in traction, and not in compression as in a generic BUS. A further difference is the inclination of the UFTs with respect to the horizontal, which leads to the necessity to enable each UFTs to continually re-orient itself in order to avoid spurious components on it. This re-orientation movement can be obtained using a couple of elastic hinges at both ends of every UFT. In our case, due to dimensional limitations, the use of elastic hinges is not possible, and spherical joints (figure 3b) were used.

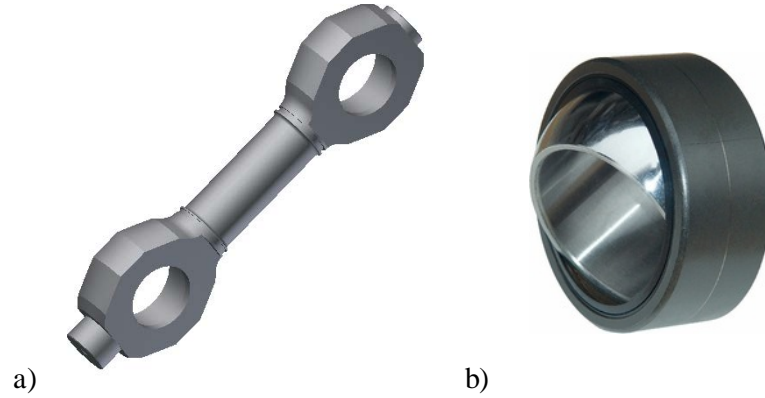


Figure 3: a) uniaxial force transducer (UFT), b) spherical joint

The force will be carried out to every single UFT through plugs passing among the plate and the spherical joints. Any deformation under load, generates a rotation moment along the axis of the spherical joint. This rotation theoretically allows the re-alignment of the whole hexapod in order to avoid any application of bending moments and or spurious components to the single UFTs. Unfortunately the rotation of the spherical joints is subjected to the friction due to the applied force. For low value of force applied, the rotation moment result higher than the friction, and the UFT is able to rotate, while for higher values of force the friction becomes more and more relevant, until it is comparable with the rotation moment, generating spurious components due to the flecion. For this reason, it is necessary that all UFTs are provided with measuring bridges properly compensated. Furthermore, the deflections of the UFTs under the load could effects the geometry of the HSM-BUS, in particular the angle formed by a pair of UFTs. In our analysis, these deflections will be treated inside the FEM analysis of the re-orientation of the UFTs.

### 2.4 Signal outputs

The measurement of the force ( $F_x, F_y, F_z$ ) and moment ( $M_x, M_y, M_z$ ) vectors are obtained combining the outputs ( $O_i$ ) of each UFT in respect to the geometry of the hexapod MFT.

The applied force tensor is conveyed and subdivided into six different forces ( $F_1, \dots, F_6$ ), each one acting and measured by each single UFT, as shown in equations (1).

$$\begin{aligned}
 F_x &= [(F_6 - F_5) - (F_2 - F_1)] \cos \beta \cos \delta \\
 F_y &= -(F_4 - F_3) \cos \beta - (F_5 - F_6) \cos \beta \cos \gamma - (F_1 - F_2) \cos \beta \cos \gamma \\
 F_z &= (F_1 + F_2 + F_3 + F_4 + F_5 + F_6) \cos \frac{\alpha}{2} \\
 M_x &= [(F_1 + F_2) - (F_5 - F_6)] 2r \cos \frac{\alpha}{2} \cos \delta \\
 M_y &= -(F_4 + F_3)r \cos \frac{\alpha}{2} + (F_1 + F_2)r \cos \frac{\alpha}{2} \sin \delta + (F_5 + F_6)r \cos \frac{\alpha}{2} \sin \delta \\
 M_z &= (F_1 - F_2 + F_3 - F_4 + F_5 - F_6)r \cos \beta
 \end{aligned} \tag{1}$$

In the above formulas,  $\alpha$ ,  $\beta$ ,  $\gamma$  and  $\delta$ , are the nominal angles related to each UFT although different values will be evaluated in practice.

In the same way, it is possible to calculate the single forces ( $F_i$ ) from the applied forces and moment vectors, as shown in equations (2)

$$\begin{aligned}
F_1 &= \frac{F_x}{4 \cos \beta \cos \delta} + \frac{F_y}{3 \cos \beta \cos \gamma} + \frac{F_z}{6 \cos \frac{\alpha}{2}} + \frac{F_x}{8r \cos \delta \cos \frac{\alpha}{2}} + \frac{F_y}{12r \sin \delta \cos \frac{\alpha}{2}} + \frac{F_z}{6r \cos \beta} \\
F_2 &= -\frac{F_x}{4 \cos \beta \cos \delta} - \frac{F_y}{3 \cos \beta \cos \gamma} + \frac{F_z}{6 \cos \frac{\alpha}{2}} + \frac{F_x}{8r \cos \delta \cos \frac{\alpha}{2}} + \frac{F_y}{12r \sin \delta \cos \frac{\alpha}{2}} - \frac{F_z}{6r \cos \beta} \\
F_3 &= -\frac{F_y}{3 \cos \beta \cos \gamma} + \frac{F_z}{6 \cos \frac{\alpha}{2}} - \frac{F_y}{12r \sin \delta \cos \frac{\alpha}{2}} + \frac{F_z}{6r \cos \beta} \\
F_4 &= \frac{F_y}{3 \cos \beta \cos \gamma} + \frac{F_z}{6 \cos \frac{\alpha}{2}} - \frac{F_y}{12r \sin \delta \cos \frac{\alpha}{2}} - \frac{F_z}{6r \cos \beta} \\
F_5 &= -\frac{F_x}{4 \cos \beta \cos \delta} + \frac{F_y}{3 \cos \beta \cos \gamma} + \frac{F_z}{6 \cos \frac{\alpha}{2}} - \frac{F_x}{8r \cos \delta \cos \frac{\alpha}{2}} + \frac{F_y}{12r \sin \delta \cos \frac{\alpha}{2}} + \frac{F_z}{6r \cos \beta} \\
F_6 &= \frac{F_x}{4 \cos \beta \cos \delta} - \frac{F_y}{3 \cos \beta \cos \gamma} + \frac{F_z}{6 \cos \frac{\alpha}{2}} - \frac{F_x}{8r \cos \delta \cos \frac{\alpha}{2}} + \frac{F_y}{12r \sin \delta \cos \frac{\alpha}{2}} - \frac{F_z}{6r \cos \beta}
\end{aligned} \tag{2}$$

### 3 Uncertainty budget

#### 3.1 General considerations

As already seen, one of the most important features of the HSM-BUS, is that, as shown by Equation (1), measurements of  $F_i$  can be directly related to the calibrated UFTs outputs  $O_i$ , from which the forces  $F_i$  are evaluated, and to the angles  $\alpha$ ,  $\beta$ ,  $\gamma$  and its complementary angle  $\delta$ . An a priori evaluation of the uncertainty can be made directly from the construction drawings, considering the geometrical tolerances. Hereafter, taking Equations (1) as mathematical models and considering the variabilities of all the independent variables, i.e. the geometry of the system and the forces measured by the UFTs, following the ISO GUM [10] the expected uncertainty can be evaluated.

#### 3.2 Valuation of the functional angles $\alpha$ and $\beta$

The forces and moments measured by the HSM-BUS are a combination of the forces measured by the single UFTs, multiplied by sine and/or cosine of relevant angles, among which two of them, denominated  $\alpha$  and  $\beta$ , can be obtained by the nominal dimensions on the technical drawings, and their variability from tolerances. Starting from the design of the upper plate, it is possible to find the distance among the axes of the two holes provided for the positioning of the UFT: this distance, at which we will refer as  $s$ , is equal to  $(467,06 \pm 0,05)$  mm. The same distance, in the lower plate, from now  $t$ , is equal to  $(166,00 \pm 0,05)$  mm; these two variables are well shown in the image below.

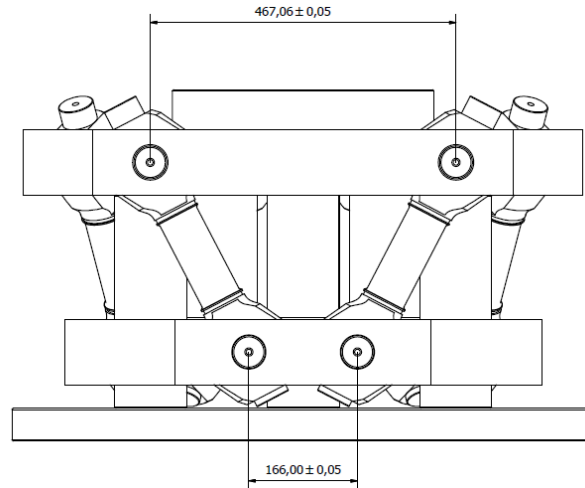


Figure 4: front view of the HSM-BUS

To complete this ideal trapezoid, it is necessary to know the length of the two oblique sides, indicated as  $d$ , which in this case is the length of the UFTs. The distance of the axes of the two holes in a UFT is equal to  $(326,00 \pm 0,02)$  mm.

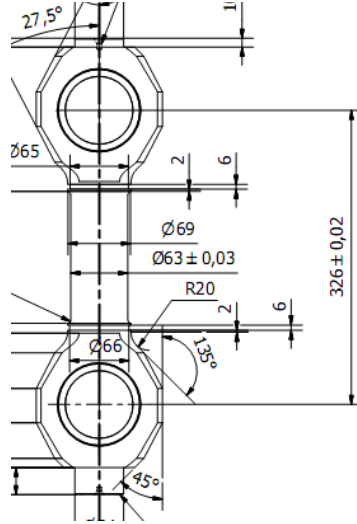


Figure 5: UFT dimension lines

In Table 1 the sides of the ideal trapezoid, with the relevant values and tolerances, are shown.

Table 1: sides of the ideal trapezoid

Side	Symbol	Value/m	Tolerance/m
upper base	$s$	$4,6706 \times 10^{-1}$	$0,0005 \times 10^{-1}$
lower base	$t$	$1,6600 \times 10^{-1}$	$0,0005 \times 10^{-1}$
diagonal	$d$	$3,2600 \times 10^{-1}$	$0,0002 \times 10^{-1}$

To evaluate the functional angles ( $\alpha$  and  $\beta$ ) we can use the following equations:

$$\begin{aligned}\alpha &= 2 \cdot \sin^{-1} \left( \frac{s-t}{2 \cdot d} \right) \\ \beta &= \cos^{-1} \left( \frac{s-t}{2 \cdot d} \right)\end{aligned}\quad (3)$$

and the results are summarized in Table 2.

Table 2: nominal values of the functional angles

Angles	Values/rad	Values/°
$\alpha$	$9,60 \times 10^{-1}$	55,0
$\beta$	$1,09 \times 10^0$	62,5

### 3.3 Evaluation of the contributions to the uncertainty of $\alpha$ and $\beta$

Equations (3) are the mathematical model used to evaluate the contributions to the uncertainty of the functional angles. For each side of the ideal trapezoid, using the respective tolerance coming from Table 1, it is possible to evaluate the relevant standard uncertainty (considering a rectangular pdf between the  $\pm a_i$ ), referred as  $u(x_i)$  and

then the sensibility coefficient  $c_i$ , as the ratio of the incremental variations; at the end, we obtained the specific contribution to the standard uncertainty  $u_i(\alpha)$  and  $u_i(\beta)$ . Table 3 and Table 4 are shown as an example of the calculation made to evaluate the relative standard uncertainty.

Table 3: equivalent variance of the independent variables

Variable	Value/m	$a_i/m$	$u(x_i)/m$
$s$	$4,6706 \times 10^{-1}$	$5 \times 10^{-5}$	$2,89 \times 10^{-5}$
$t$	$1,6600 \times 10^{-1}$	$5 \times 10^{-5}$	$2,89 \times 10^{-5}$
$d$	$3,2600 \times 10^{-1}$	$2 \times 10^{-5}$	$1,15 \times 10^{-5}$

The standard uncertainty of each variable is described as a parameter of category B with cautelatively 30 degree of freedom.

From the equivalent variance is possible to calculate the contribution to the standard uncertainty of the functional angles using the appropriate sensibility coefficients,  $c_i$ .

Table 4: calculation of the contributions to the relative standard uncertainty of the functional angles

Variable	$c_i(\alpha)$	$u_i(\alpha)$	$c_i(\beta)$	$u_i(\beta)$
$s$	$3,5 \times 10^0$	$9,98 \times 10^{-5}$	$-1,73 \times 10^0$	$4,99 \times 10^{-5}$
$t$	$-3,5 \times 10^0$	$9,98 \times 10^{-5}$	$1,73 \times 10^0$	$4,99 \times 10^{-5}$
$d$	$-3,2 \times 10^0$	$3,69 \times 10^{-5}$	$1,60 \times 10^0$	$1,84 \times 10^{-5}$

In Table 5 the standard uncertainties of the functional angles  $\alpha$  and  $\beta$  obtained by the above calculation are shown.

Table 5: standard uncertainties of the functional angles

Angle	$u_{fa}/\text{rad}$
$\alpha$	$1,5 \times 10^{-4}$
$\beta$	$7,3 \times 10^{-5}$

### 3.4 Analysis of the tolerances

The above calculations regard only the quotes lines variation in the XY plane, supposing that all the geometry would be parallel (or perpendicular) to the Z-axis. Therefore, we have to investigate the effect of an undesired inclination, respect to the Z-axis, due to the construction tolerances of the MFT. In addition, we have to consider other two ideal geometrical elements: the vertical distance between the two plates, that we will call  $l$ , and the maximum misalignment of the face of the plates, indicated as  $m$ . They are obtained as the sum of the tolerances of the distances between the faces of the plates and the centre in which passes the axis of symmetry of the HSM-BUS. All the elements necessary to our calculations are summarized in Table 6.

Table 6: list of the ideal geometrical elements

Variable	Symbol	Value/m
vertical distance	$l$	$2,89 \times 10^{-1}$
maximum misalignment	$m$	$8,00 \times 10^{-5}$
upper base	$s$	$4,6706 \times 10^{-1}$
lower base	$t$	$1,6600 \times 10^{-1}$

The half widths of the functional angles ( $\alpha$  and  $\beta$ ) are so defined:

$$\rho = \frac{1}{2} \tan^{-1} \left( \frac{m}{l} \right) \quad (4)$$

To complete the contribution to the uncertainty of the HSM-BUS geometry, we need to analyze other two complementary angles,  $\gamma$  and  $\delta$ , as seen in Fig. 1; their half width is defined as:

$$\phi = \tan^{-1} \left( \frac{m}{t} \cdot \frac{t+s}{s-t} \right) \quad (5)$$

The values of the two half width intervals above defined are represented in Table 7.

Table 7: half width intervals

Angle	Value/rad
$\rho$	$1,4 \times 10^{-4}$
$\phi$	$1,0 \times 10^{-3}$

This means that, for the two functional angles  $\alpha$  and  $\beta$ , the total contribution to the uncertainty is given by:

$$u_{tot} = \sqrt{(u_{fa})^2 + \frac{\rho^2}{3}} \quad (6)$$

and the total contributions to the uncertainty of all the four angles are:

Table 8: total contribution to the uncertainty of the angles

Angles	$u_{tot}/\text{rad}$
$\alpha$	$1,8 \times 10^{-4}$
$\beta$	$1,1 \times 10^{-4}$
$\gamma$	$1,0 \times 10^{-3}$
$\delta$	$1,0 \times 10^{-3}$

### 3.5 UFT Calibration

The calibration of the single UFTs is one important contribution to the uncertainty budget of the HSM-BUS. The calibration procedure is conform to the UNI EN ISO 376 [11], and can be summarized as:

- Two loading phases at initial position (indicated as  $0^\circ$ ), only with incremental force values
- Two other loading phases with relative rotation of the position (approximately  $120^\circ$  and  $240^\circ$ ) with incremented and decremented force values

The values obtained are then evaluated fitting the calibration data with a linear regression with equation:

$$y = a + b \times x + c \times x^2 + d \times x^3 \quad (7)$$

Every single UFT has its respective fitting equation that is used to convert the signal output into a force signal. Since the calibration of the UFTs are not yet done, but taking into account that for a metrological use of the MFT it is necessary to choose UFTs with the lower uncertainty possible, for our calculation we had considered UFTs classified in class 00 [11] that corresponds to a maximum relative uncertainty of  $6 \times 10^{-4}$ .



### 3.6 Uncertainty budget

These calculations are made considering an unmodified geometry under loads. With all the evaluated contributions to the uncertainty budget, it is now possible to estimate the budget of uncertainty of the signal output of the HSM-BUS. We had considered the uncertainty for each type of signal output ( $F_z$ ,  $F_x$ ,  $F_y$ ,  $M_z$ ,  $M_x$ ,  $M_y$ ), but for simplicity we show only the estimation of uncertainty of the axial force  $F_z$ .

From equations (1) we see that the axial force is obtained by:

$$F_z = F_1 \cos\left(\frac{\alpha_1}{2}\right) + F_2 \cos\left(\frac{\alpha_2}{2}\right) + F_3 \cos\left(\frac{\alpha_3}{2}\right) + F_4 \cos\left(\frac{\alpha_4}{2}\right) + F_5 \cos\left(\frac{\alpha_5}{2}\right) + F_6 \cos\left(\frac{\alpha_6}{2}\right) \cong (F_1 + F_2 + F_3 + F_4 + F_5 + F_6) \cos\left(\frac{\alpha}{2}\right) \quad (8)$$

We can now evaluate the contributions to the relevant standard uncertainty due to the forces measured by the single UFTs and due to the angles, resumed in Table 9.

Table 9: contributions to the combined relative standard uncertainty for  $F_z$  at full load

Parameter	$u(x_i)$	$c_i$	$u_i(F_z)/\text{kN}$	$u_i(F_z)_{\text{rel}}$
$F_{(1,2,3,4,5,6)}$	$2.82 \times 10^{-1} \text{ kN}$	$8.87 \times 10^{-1}$	$2.50 \times 10^{-1}$	$5.00 \times 10^{-5}$
$\alpha$	$1.63 \times 10^{-4} \text{ rad}$	$-1.30 \times 10^3$	$2.13 \times 10^{-1}$	$4.25 \times 10^{-5}$

The contributions to the combined relative standard uncertainty have been evaluated taking into account type A and B standard uncertainties, and have been combined following the ISO GUM [10] guide lines.

From the calculations, the relative expanded uncertainty of  $F_z$  is equal to  $2.68 \times 10^{-4}$ . It is very important to observe that the contributions due to the functional angle  $\alpha$  and to the force measurement have about the same weight into the expanded uncertainty budget of  $F_z$ .

For the other two components of the force vector, we report briefly the respective calculation of the contributions to the relative standard uncertainty.

Table 10: contributions to the relative standard uncertainty for  $F_x$ , evaluated at the level of 100 kN

Parameter	$u(x_i)$	$c_i$	$u_i(F_x)/\text{kN}$	$u_i(F_x)_{\text{rel}}$
$F_{\text{output}(1,2,5,6)}$	$1.88 \times 10^{-2} \text{ kN}$	$4.00 \times 10^{-1}$	$7.50 \times 10^{-3}$	$7.50 \times 10^{-5}$
$\beta$	$5.69 \times 10^{-5} \text{ rad}$	$-1.92 \times 10^2$	$1.09 \times 10^{-2}$	$1.09 \times 10^{-4}$
$\delta$	$2.89 \times 10^{-4} \text{ rad}$	$-5.77 \times 10^1$	$1.67 \times 10^{-2}$	$1.67 \times 10^{-4}$

Table 11: contributions to the relative standard uncertainty for  $F_y$ , evaluated at the level of 100 kN

Parameter	$u(x_i)$	$c_i$	$u_i(F_y)/\text{kN}$	$u_i(F_y)_{\text{rel}}$
$F_{\text{output}(1,2,5,6)}$	$1.08 \times 10^{-2} \text{ kN}$	$-2.31 \times 10^{-1}$	$2.50 \times 10^{-3}$	$2.50 \times 10^{-5}$
$F_{\text{output}(3,4)}$	$2.17 \times 10^{-2} \text{ kN}$	$4.62 \times 10^{-1}$	$1.00 \times 10^{-2}$	$1.00 \times 10^{-4}$
$\beta$	$8.04 \times 10^{-5} \text{ rad}$	$-1.92 \times 10^2$	$1.54 \times 10^{-2}$	$1.54 \times 10^{-4}$
$\gamma$	$5.77 \times 10^{-4} \text{ rad}$	$-5.77 \times 10^1$	$2.36 \times 10^{-2}$	$2.36 \times 10^{-4}$

In these cases, we can observe that the most significant contributions to the expanded uncertainty are coming from the angles, especially from the complementary ones ( $\delta$  and  $\gamma$ ). As the same way for the force vector, we have evaluated the uncertainty of the components of the moment vectors; below are briefly shown the calculation of the contributions to the relative standard uncertainty.

Table 12: contributions to relative standard uncertainty for  $M_z$ , evaluated at the level of 100 kN·m and full load for  $F_z$

Parameter	$u(x_i)$	$c_i$	$u_i(M_z)/\text{kN}\cdot\text{m}$	$u_i(M_z)$
-----------	----------	-------	-----------------------------------	------------

$F_{output(1,3,5)}$	$3.32 \times 10^{-1}$ kN	$9.93 \times 10^{-2}$	$3.30 \times 10^{-2}$	$3.30 \times 10^{-4}$
$F_{output(2,4,6)}$	$2.31 \times 10^{-1}$ kN	$-9.93 \times 10^{-2}$	$2.30 \times 10^{-2}$	$2.30 \times 10^{-4}$
$r$	$2.89 \times 10^{-5}$ m	$4.65 \times 10^2$	$1.34 \times 10^{-2}$	$1.34 \times 10^{-4}$
$\beta$	$4.64 \times 10^{-5}$ rad	$-1.92 \times 10^2$	$8.92 \times 10^{-3}$	$8.92 \times 10^{-5}$

Table 13: contributions to the relative standard uncertainty for  $M_x$ , evaluated at the level of 100 kN·m and full load for  $F_z$

Parameter	$u(x_i)$	$c_i$	$u_i(M_x)/\text{kN}\cdot\text{m}$	$u_i(M_x)$
$F_{output(1,2)}$	$3.27 \times 10^{-1}$ kN	$1.65 \times 10^{-1}$	$5.40 \times 10^{-2}$	$5.40 \times 10^{-4}$
$F_{output(5,6)}$	$2.36 \times 10^{-1}$ kN	$-1.65 \times 10^{-1}$	$3.90 \times 10^{-2}$	$3.90 \times 10^{-4}$
$r$	$1.44 \times 10^{-5}$ m	$4.65 \times 10^2$	$6.71 \times 10^{-3}$	$6.71 \times 10^{-5}$
$\alpha$	$8.69 \times 10^{-5}$ rad	$-2.60 \times 10^1$	$2.33 \times 10^{-3}$	$2.33 \times 10^{-5}$
$\delta$	$2.89 \times 10^{-4}$ rad	$-5.77 \times 10^1$	$1.67 \times 10^{-2}$	$1.67 \times 10^{-4}$

Table 14: contributions to the relative standard uncertainty for  $M_y$ , evaluated at the level of 100 kN·m and full load for  $F_z$

Parameter	$u(x_i)$	$c_i$	$u_i(M_y)/\text{kN}\cdot\text{m}$	$u_i(M_y)$
$F_{output(1,2,5,6)}$	$3.08 \times 10^{-1}$ kN	$9.54 \times 10^{-2}$	$2.94 \times 10^{-2}$	$2.94 \times 10^{-4}$
$F_{output(3,4)}$	$2.29 \times 10^{-1}$ kN	$-1.91 \times 10^{-1}$	$4.38 \times 10^{-2}$	$4.38 \times 10^{-4}$
$r$	$2.04 \times 10^{-5}$ m	$4.65 \times 10^2$	$9.49 \times 10^{-3}$	$9.49 \times 10^{-5}$
$\alpha$	$1.27 \times 10^{-4}$ rad	$-2.60 \times 10^1$	$3.30 \times 10^{-3}$	$3.30 \times 10^{-5}$
$\delta$	$4.08 \times 10^{-4}$ rad	$6.78 \times 10^2$	$2.77 \times 10^{-1}$	$2.77 \times 10^{-3}$

Now we can show the uncertainty for each component of the force vector and of the moment vector:

Table 15: relative expanded uncertainty of the force and moment components

Component	$U(y)$
$F_z$	$2.56 \times 10^{-4}$
$F_x$	$5.09 \times 10^{-4}$
$F_y$	$6.52 \times 10^{-4}$
$M_z$	$1.46 \times 10^{-3}$
$M_x$	$1.96 \times 10^{-3}$
$M_y$	$5.92 \times 10^{-3}$

## 4 Data simulation

### 4.1 Introduction

We have theorized that the application of the loads does not affect the geometry of the system. In the last part of our analysis, simulating the HSM-BUS under loads, we have verified the amplitude of these variations in order to evaluate if they are significant or negligible.

In the previous paragraphs it was discussed how, during the entire loading process, the single UFT needs to modify the initial angles, so it is necessary to verify how much these angle variations are and in which term they modify the force measurements. With the use of a FEM simulation, we have studied the variation of the position of the HSM-BUS elements in the space, in order to evaluate the different angle values during the loading process.

### 4.2 Angle values evaluation

The measure of the angle under the load application can be obtained from simple geometrical calculation. We have simulated the deformation of the system at seven different loads and we focused our attention on two points, A and B, as shown in figure 6.

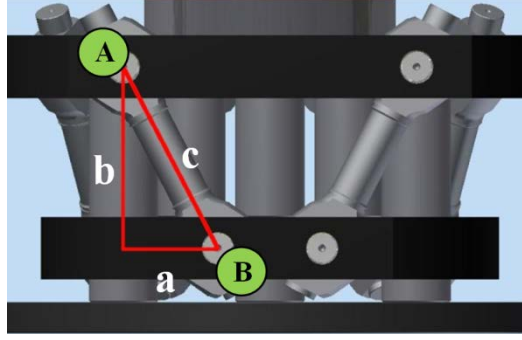


Figure 6: The imaginary triangle created by points A and B.

These two points create an imaginary triangle, so the angle  $\eta$ , i.e. the complementary angle of  $\beta$  and equal to  $\alpha/2$ , can be obtained from the variations on Z-direction and X-direction using the equation (9).

$$\eta = \cos^{-1}\left(\frac{b'}{c'}\right) = \cos^{-1}\left(\frac{b+\delta z}{\sqrt{(b+\delta z)^2+(a+\delta x)^2}}\right) \quad (9)$$

Thanks to the orientation of the hexapod in the coordinates system, the variation on the Y-direction does not influence the angle  $\eta$ , so we can easily neglect it.

#### 4.3 First simulation

In order to simplify the model, in our first simulation, we neglected also the variation on the X-direction, so (9) became:

$$\eta = \cos^{-1}\left(\frac{b'}{c'}\right) \sim \cos^{-1}\left(\frac{b+\delta z}{\sqrt{(b+\delta z)^2+a^2}}\right) \quad (10)$$

and we obtain the values in Table 16.

Table 16: Angle values simulated under load

Force/kN	$\delta A/\text{mm}$	$\delta B/\text{mm}$	$\cos \eta$	$\alpha/^\circ$
200	-0,029	-0,040	0,88706	54,99
500	-0,073	-0,100	0,88707	54,99
1000	-0,145	-0,201	0,88709	54,98
2000	-0,290	-0,402	0,88712	54,97
3000	-0,435	-0,602	0,88716	54,96
4000	-0,580	-0,803	0,88720	54,95
5000	-0,725	-1,004	0,88723	54,95

At this point, we compare the difference on the force calculated with the theoretical angle ( $55^\circ$ ) and with the simulated ones, obtaining the results in Table 17.

Table 17: Theoretical values vs. simulated values of the force

Theor. force/kN	Theor. $\alpha/^\circ$	Simul. $\alpha/^\circ$	Sim. force/kN	Rel. diff. $\Delta$
200	55	54,99	199,99	$5,1 \times 10^{-5}$
500	55	54,99	499,97	$6,3 \times 10^{-5}$
1000	55	54,98	999,92	$8,4 \times 10^{-5}$
2000	55	54,97	1999,75	$1,3 \times 10^{-4}$
3000	55	54,96	2999,50	$1,7 \times 10^{-4}$
4000	55	54,95	3999,17	$2,1 \times 10^{-4}$
5000	55	54,95	4998,76	$2,5 \times 10^{-4}$

The relative differences, i.e. the possible errors generated by the deformation of HSM-BUS under load, resulting from the above calculation are significant considering the use of MTF for our applications. Therefore, we have investigated the possibility to modify our equations taking into account the variation of the angle values under load. Therefore, we have calculated a first order polynomial interpolated equation (11) through a linear regression of the simulated values, i.e.

$$2\eta = a + b \cdot F \quad (11)$$

where  $a = 54,99056(\pm 0,00003)$  and  $b = -9,05(\pm 0,01) \times 10^{-6}$ .

Now, the comparison of the theoretical force with the simulated and corrected ones gives us the results shown in Table 18.

Table 18: Simulated values vs. corrected values

Theor. force/kN	Simul. $\alpha/^\circ$	Corr. $\alpha/^\circ$	Corr. force/kN	Rel. diff., $\Delta_{sim}$	Rel. diff., $\Delta_{corr}$
200	54,98875	54,9887	200,000003	$5,1 \times 10^{-5}$	$-1,3 \times 10^{-8}$
500	54,98603	54,9860	499,999981	$6,3 \times 10^{-5}$	$3,8 \times 10^{-8}$
1000	54,98150	54,9815	999,999941	$8,4 \times 10^{-5}$	$5,9 \times 10^{-8}$
2000	54,97247	54,9725	1999,999966	$1,3 \times 10^{-4}$	$1,7 \times 10^{-8}$
3000	54,96346	54,9634	3000,000552	$1,7 \times 10^{-4}$	$-1,8 \times 10^{-7}$
4000	54,95439	54,9544	4000,000119	$2,1 \times 10^{-4}$	$-3,0 \times 10^{-8}$
5000	54,94531	54,9453	4999,999439	$2,5 \times 10^{-4}$	$1,1 \times 10^{-7}$

It is easy to see that this correction theoretically allow reducing at a negligible level the expected errors due to mechanical distortions.

#### 4.4 Final simulation

At this point, we have verified if it is correct to neglect the effect on the angle values given by the variation on the X-direction. Therefore, at the load of 5 MN, we have compared the theoretical force with the simulated forces derived from the angle  $\eta$  computed using the equations (9) and (10). As results, we have obtained significant differences in the results, showing that the effect of the position variation on the X-direction cannot be neglected. Therefore, we have recalculated all the angle values taking into account both the Z-direction as the X-direction variations. The difference on the angle values are shown in figure 9.

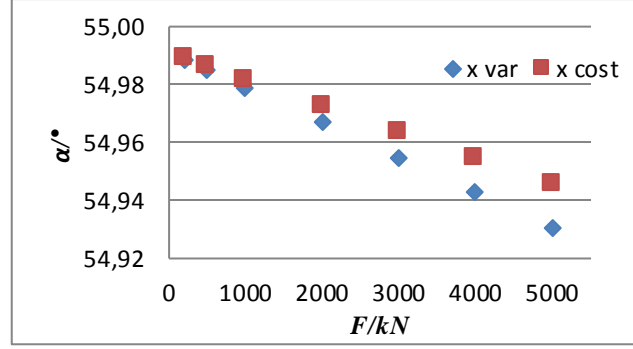


Figure 7: Angle values calculated with  $x$  variable (equation 10) and constant (equation 9).

As before, we calculated a fitting curve using a linear regression of all the angle values simulated in order to provide the angle values for all possible loads conditions, obtaining a nearly linear pattern of the values, as shown in Table 19:

Table 19: Simulated values vs corrected values

Theor. force/kN	Simul. $\alpha/^\circ$	Calc. $\alpha/^\circ$	Calc. force/kN	Rel. Diff., $\Delta corr$
200	54,98815	54,9881	199,989	$-3,9 \times 10^{-8}$
500	54,98455	54,9845	499,965	$-2,2 \times 10^{-8}$
1000	54,97852	54,9785	999,902	$6,2 \times 10^{-8}$
2000	54,96651	54,9665	1999,696	$7,2 \times 10^{-8}$
3000	54,95455	54,9545	2999,381	$-1,5 \times 10^{-7}$
4000	54,94248	54,9425	3998,956	$1,2 \times 10^{-7}$
5000	54,93051	54,9305	4998,423	$-4,5 \times 10^{-8}$

## 5 Final uncertainty budget

### 5.1 Enhanced mathematical model

From the previous calculation, we have seen that it is necessary to take into account a correction  $\Delta\alpha$  to the functional angle  $\alpha$  and that the model considering the variation into the two directions X and Z is the best. This correction, as a function of the applied nominal force  $F$ , is described by:

$$\Delta\alpha = a + b \cdot F \quad (12)$$

and has the following parameter:

Table 20: Parameter of the correction  $\Delta\alpha$

Parameter	Value	$u(x_i)$
$a$	$-9,45 \times 10^{-3} \text{ }^\circ$	$1,39 \times 10^{-5} \text{ }^\circ$
$b$	$-1,20 \times 10^{-5} \text{ }^\circ/\text{kN}$	$4,94 \times 10^{-9} \text{ }^\circ/\text{kN}$

The functional angle  $\alpha$  presents in equations (1) must be corrected as  $\alpha + \Delta\alpha$ .

### 5.2 Enhanced uncertainty budget

Now we have to verify if it necessary to re-evaluate the uncertainty on the force and moment components, since there is a new contribution to take into account. As an example, we have done the calculation on the expanded uncertainty of  $F_z$ , which is obtained modifying equations (1) with equation (12):

$$F_z = (F_1 + F_2 + F_3 + F_4 + F_5 + F_6) \cos\left(\frac{\alpha + \Delta\alpha}{2}\right) \quad (13)$$

The contributions to the relative standard uncertainty are shown below:

Table 21: contributions to the relative standard uncertainty

Parameter	$u(x_i)$	$c_i$	$u_i(F_z)$
$F_{output}$	$5,64 \times 10^{-5}$	$8,87 \times 10^{-1}$	$5,00 \times 10^{-5}$
$a$	$2,78 \times 10^{-9}$	$-2,27 \times 10^1$	$6,30 \times 10^{-8}$
$b$	$9,88 \times 10^{-13}$	$-1,13 \times 10^5$	$1,12 \times 10^{-7}$
$F$	$4,78 \times 10^{-8}$	$2,72 \times 10^{-4}$	$1,30 \times 10^{-11}$
$\alpha$	$3,59 \times 10^{-8}$	$-1,30 \times 10^3$	$4,66 \times 10^{-5}$

As can be easily seen, the contributions to the uncertainty budget due to the correctional factor are much lower than others higher contributions, so they do not increase significantly the total uncertainty.

### 5.3 Possible enhancements of the uncertainty budget

The calculation seen above are referred to the tolerances given in the technical drawing. Therefore, the uncertainty can be reduced by measuring accurately the real geometry and using UFTs with a lower uncertainty. The goal of the project is to use the new 5 MN MFT as a 5 MN force reference transducer with internal traceability, for replacing the present one, which must be calibrated externally and has a uncertainty of  $5 \times 10^{-4}$ . To reach this level of uncertainty, is possible to use UFTs in class 00 [11], that allows a maximum expanded uncertainty of  $6 \times 10^{-4}$ , that would lead a relative uncertainty of  $2,7 \times 10^{-4}$  on the axial force output ( $F_z$ ).

## 6 CONCLUSIONS

The 5 MN Hexapod-Shaped Multicomponent Build-Up System (HSM-BUS) can represent a calculated standard, taking traceability within INRIM force laboratory. From the present study result possible to obtain the required measurement accuracy with the proposed HSM-BUS just using the geometrical tolerances prescribed for the mechanical construction. Being the angle effects the main contributions to uncertainty, it is necessary a high level, metrological measurement of the geometry of the system to enhance the accuracy. The use of UFTs in class 00 [11] can also help.

The simulation of the HSM-BUS behaviors under load had shown the necessity to estimate the variation of the functional angle  $\alpha$  for each UFT. It can be a source of a significant error and shall be taken into account in the calculation process.

The metrological characterization of the new 5MN HSM-BUS is obtained by three different procedures, i.e. the calibration of each UFT, the measurement of the system geometry and the evaluation of the functional angle  $\alpha$  under load.

The next step will be the realisation of the new 5 MN HSM-BUS and the its comparison with the actual 5 MN uniaxial force reference transducer.

## ACKNOWLEDGMENTS

The activity of these research has been carried out in the framework of the EMRP Joint Research Project SIB63 “Force” with the title “Force traceability within the meganewton range”, WP2 [12].

The EMRP is jointly funded by the EMRP participating countries within EURAMET and the European Union.

## REFERENCES

- [1] J.Cruz, V.Prodonoff, J.Guerhard, “Research, Development and Characterization of a Build-up System Prototype up to 600 kN”, *XVII IMEKO World Congress*, Istanbul, Turkey, Sept. 2001.
- [2] Li Qingzhong, Yao Jinhui, Xu Hang, Li Haigen, Li Ting yuan, “10 MN build-up force standard machine developed in China”, *IMEKO World Congress*, Pattaya, Thailand, Nov. 2010.
- [3] Yao Jinhui, Li Qingzhong, Xu Hang, Chi Hui, Lin jianhui, Li Haigen, “Design of 60 MN Build-up Force Standard machine”, *XXII IMEKO World Congress*, Cape Town, Republic of South Africa, Feb. 2014.
- [4] Bariş ÇAL, Sinan FANK, Hakan Ö. ÖZBAY, Ercan PELİT, Cihan KUZU, Bülent AYDEMİR, “3 MN hydraulic type build-up force standard machine installed at National Metrology Institute (UME)”, *XVII IMEKO World Congress*, Dubrovnik, Croatia, Sept. 2003.
- [5] Dae-Im Kang, Hou-Keun Song, Jeong-Tae Lee, You-Kyu Park and Jong-Ho Kim, “Traceability of large force standards in Korea”, *XVII IMEKO World Congress*, Dubrovnik, Croatia, Sept. 2003.
- [6] C. Ferrero, C. Marinari, E. Martino, “Development and metrological characterisation of a build-up force standard up to 3 MN”, *XVII IMEKO World Congress*, Dubrovnik, Croatia, Sept. 2003.
- [7] Gerhard Schulder, Ulrich Kolwinski, Daniel Schwind, “A new design of a 5,4 MN build-up system”, *XVIII IMEKO World Congress*, Rio de Janeiro, Brazil, Sept. 2006.
- [8] Sergio Desogus, Alessandro Germak, Fabrizio Mazzoleni, Danilo Quagliotti, Giulio Barbato, Arturo Barbieri, Giacomo Bigolin, Carlo Bin, “Developing multicomponent force transducers at INRiM”, *IMEKO World Congress*, Pattaya, Thailand, Nov. 2010.
- [9] Gianfranco Genta, Alessandro Germak, “Metrological characterization of an hexapod-shaped multicomponent force transducer”, *IX NATIONAL GROUP OF MECHANICAL AND THERMAL MEASUREMENTS Congress*, Ancona, Italy, Sept. 2014.
- [10] JCGM 100:2008, “Evaluation of measurement data - Guide to the expression of uncertainty in measurement (GUM)”.
- [11] UNIEN ISO 376, "Calibration of force-proving instruments used for the verification of uniaxial testing machines", Jun. 1999.
- [12] R. Kumme, F.Tegtmeier, D. Röske, A. Barthel, A. Germak and P. Averlant, “Force traceability within the meganewton range”, *XXII IMEKO World Congress*, Cape Town, Republic of South Africa, Feb. 2014.